Appl Nanosci (2016) 6:827–836
DOI 10.1007/s13204-015-0501-z

ORIGINAL ARTICLE

Preliminary protein corona formation stabilizes gold nanoparticles and improves deposition efficiency

Alexandra O. Luby[1] · Emily K. Breitner[1] · Kristen K. Comfort[1]

Received: 11 May 2015 / Accepted: 14 September 2015 / Published online: 24 September 2015

Abstract Due to their advantageous characteristics, gold nanoparticles (AuNPs) are being increasingly utilized in a vast array of biomedical applications. However, the efficacy of these procedures are highly dependent upon strong interactions between AuNPs and the surrounding environment. While the field of nanotechnology has grown exponentially, there is still much to be discovered with regards to the complex interactions between NPs and biological systems. One area of particular interest is the generation of a protein corona, which instantaneously forms when NPs encounter a protein-rich environment. Currently, the corona is viewed as an obstacle and has been identified as the cause for loss of application efficiency in physiological systems. To date, however, no study has explored if the protein corona could be designed and advantageously utilized to improve both NP behavior and application efficacy. Therefore, we sought to identify if the formation of a preliminary protein corona could modify both AuNP characteristics and association with the HaCaT cell model. In this study, a corona comprised solely of epidermal growth factor (EGF) was successfully formed around 10-nm AuNPs. These EGF-AuNPs demonstrated augmented particle stability, a modified corona composition, and increased deposition over stock AuNPs, while remaining biocompatible. Analysis of AuNP dosimetry was repeated under dynamic conditions, with lateral flow significantly disrupting deposition and the nano-cellular interface. Taken together, this study demonstrated the plausibility and potential of utilizing the protein corona as a means to influence NP behavior; however, fluid dynamics remains a major challenge to progressing NP dosimetry.

Keywords Gold nanoparticles · Protein corona · Epidermal growth factor · Deposition · Dynamic flow

Introduction

In recent years, colloidal gold nanoparticles (AuNPs) have attracted significant attention for use in biomedical applications. For example, research is underway to develop AuNP-based procedures for drug and gene delivery, bioimaging techniques, sensor systems, cancer therapeutics, and vaccine development (Dykman and Khlebtsov 2012; Stacy et al. 2013). AuNPs are viewed as advantageous over other materials for a multitude of reasons, including a general biocompatibility, standardized synthesis protocols, ease of functionalization, and distinctive plasmonic properties (Yeh et al. 2012). While biomedical applications vary in function, what they have in common is the need for a high AuNP delivery rate to be effective. Current design efforts to improve colloid delivery and deposition have focused on material-based approaches, specifically through modification of particle size or surface chemistry (Bannunah et al. 2014; Untener et al. 2013). While these efforts have been met with moderate success, much work remains to optimize NP deposition and dosimetry (Pal et al. 2015).

When nano-based biomedical applications are applied within a biological system, there exists a significant loss of effectiveness. Physiological variables have been shown to modify NP properties and behavior, providing an explanation for these discrepancies (Tenzer et al. 2013). For example, when NPs are introduced to a biological system,

✉ Kristen K. Comfort
kcomfort1@udayton.edu

[1] Department of Chemical and Materials Engineering, University of Dayton, Kettering Laboratories 524, 300 College Park, Dayton OH 45469, USA

surrounding proteins instantaneously adsorb onto their surface, generating a protein corona: which serves as the biological identify of the NPs (Gunawan et al. 2014). The protein corona is dynamic by nature with its composition dependent on numerous factors, including localized protein gradients, available biomolecules, kinetic equilibrium constants, and circulation time (Sahneh et al. 2015). The corona is comprised of two distinct layers, referred to as the hard and soft coronas. The hard corona is a single layer of proteins directly bound to the NP surface with high affinity, forming a stable coating. The soft corona, which covers the hard corona, is loosely associated and, therefore, promotes dissociation and rapid biomolecule exchange (Winzen et al. 2015). Previous studies have demonstrated that the protein corona directly impacts the nano-cellular interface, thereby determining NP deposition efficiency, membrane interactions, degree of endocytosis, and biocompatibility (Chanana et al. 2013; Lesniak et al. 2013; Treuel et al. 2014).

The protein corona has been identified as the primary source for loss of application efficacy and poor predicative modeling in complex biological systems (Salvati et al. 2013). To date, the nonspecific adsorption involved with the protein corona is typically viewed as a negative and unavoidable side effect (Hamad-Schifferli 2013). In addition to modifying the surface area to volume ratio and the nano-cellular interface, a protein–NP complex increases aggregation and introduces a level of unpredictability through the weak chemical bonds supporting this structure. While the scientific community has agreed that protein coronas are an inevitable aspect of nano-biotechnology, it has yet to be explored if generating a targeted protein corona prior to biological introduction is of benefit with regards to NP stability, dosimetry, or subsequent bioresponses.

Additionally, in vivo systems are circulatory and dynamic resulting in tissue-based biotransport. As standard in vitro models operate under static conditions, fluid dynamic variations to NP and cellular behavior are neglected in these models. Preliminary work has identified that the introduction of dynamic flow modified cellular morphology, NP behavior, and NP dosimetry (Breitner et al. 2015; Kusunose et al. 2013; Ucciferri et al. 2014). These results suggest that the nano-cellular interface and the rate of NP deposition will be influenced by dynamic flow; making it a critical variable to include during AuNP application analysis.

As such, the goal of this study was to explore if AuNP behavior and deposition efficiency could be improved through the targeted generation of a preliminary protein corona. Using 10-nm AuNPs, a protein corona comprised solely of epidermal growth factor (EGF) was formed prior to cellular exposure (EGF-AuNPs). EGF was chosen due to the fact that its receptor is predominantly expressed on most cell types, providing an opportunity for increased AuNP–cellular binding. The human keratinocyte HaCaT cell line was selected owing to its role as a model system for NP evaluations (Comfort et al. 2014a) and its documented expression of EGF receptors (Chichocki et al. 2014). Our results demonstrated altered behavior of the EGF-AuNPs versus untreated AuNPs, including stabilization of agglomerates, a larger protein corona size, and increased deposition. In an attempt to better predict AuNP delivery under realistic conditions, deposition analysis was repeated under dynamic conditions. The introduction of fluid flow altered the modes of biotransport, limiting AuNP–HaCaT interactions and reducing AuNP deposition. Taken together, these results revealed that targeted protein corona formation is capable of stabilizing AuNP behavior and improving delivery rate. However, for this process to be effectively incorporated into the design of nano-based applications, other factors, such as the presence of dynamic flow, need to be accounted for.

Experimental section

NP characterization

The 10-nm, citrate-coated AuNPs were purchased in concentrated solution form from Nanocomposix. Prior to cell exposure, the AuNPs were characterized to identify target physicochemical parameters. Transmission electron microscopy (TEM) imaging was carried out on a Hitachi H-7600. Dynamic light scattering (DLS) and zeta potential analyses were performed on a Malvern Zetasizer Nano-ZS. The spectral signature of the AuNPs was identified through UV–VIS analysis on a Varian Cary 5000. Characterization was carried out in accordance with manufacturer specifications at a concentration of 25 μg/mL.

Cell culture

The human keratinocyte cell line, HaCaT, was a kind gift from the Air Force Research Laboratories. HaCaTs were maintained in RPMI 1640 medium supplemented with 10 % fetal bovine serum (FBS) and 1 % penicillin/streptomycin at 37 °C in a humidified incubator. During experimentation, HaCaTs were seeded in 24-well plates at a concentration of 2×10^5 cells per well. All cell culture supplies were purchased from Life Technologies.

Establishment of a dynamic cellular system

Dynamic flow was introduced through the use of a 24-channel peristaltic pump (Ismatec), with each channel

connected to a single cell culture well. The pump operated with standard 1/16 inch tubing, positioned at opposite ends of each well to ensure unidirectional flow. The pump was ran at a target volumetric flowrate of 1.98×10^{-2} cm^3/s to produce average linear velocities of 1.0 and 0.01 cm/s in the tubing and across the cell surface, respectively. This flowrate was chosen to match known physiological flow patterns. To minimize the introduction of environmental variables, the entire pump system was housed within the incubator.

Protein corona establishment

FBS within the media served as the protein source to form the corona. To ensure consistency, the same FBS lot was used throughout this study. The EGF-AuNPs were formed by incubating 15 μg/mL AuNPs in excess (10 μM) solution of human recombinant EGF (Peprotech) at 4 °C. After 48 h, the EGF-coated AuNPs were recovered through centrifugation, resuspended, and either characterized or introduced to the HaCaT cells.

Protein corona identification and quantification

Following incubation of either AuNPs or EGF-AuNPs in water or media (total mass of 15 μg), the AuNPs were pelleted through centrifugation. The NPs were washed twice with phosphate-buffered saline (PBS) to remove any unattached protein, and were resuspended in 30 μL PBS. The proteins were removed from the AuNP surface by boiling for 5 min in 2× Laemmli sample buffer (Biorad), after which the NPs were again pelleted. Following removal from the AuNPs, the protein concentration was determined using DC Protein Assay (Biorad), in accordance with the manufacturer's instructions.

The protein corona was visualized through SDS-PAGE analysis. Briefly, the protein-containing supernatant was loaded onto a 4–20 % gradient mini-PROTEAN TGX gel (Biorad). Following electrophoresis, the gel was rinsed in water and dyed with Gel Code Blue (Life Technologies) for band visualization.

AuNP deposition efficiency

HaCaTs were seeded in a 24-well plate at a density of 2×10^5 cells per well and returned to the incubator overnight to ensure full adherence. Fresh dosing solutions at a concentration of 15 μg/mL of either AuNPs or EGF-AuNPs were generated and underwent UV–VIS analysis. The cells were then washed and dosed with the denoted NP set and incubated under either static or dynamic conditions for 24 h. Fluid samples were collected in triplicate and analyzed via UV–VIS to determine the final AuNP concentration (Zook et al. 2011). The change in AuNP concentration was considered the deposited dose.

HaCaT viability assessment

HaCaT cells were seeded in 24-well plates at a density of 2×10^5 cells per well and incubated for 24 h to allow for full adherence. Next, they were dosed with 15 μg/mL of the denoted AuNPs for a duration of 24 h, after which cell viability was assessed using the CellTiter 96 Aqueous One Solution (Promega) in accordance with the manufacturer's specifications. HaCaTs that were untreated served as the negative control for normalization.

Cellular internalization

For visualization of AuNP internalization, TEM imaging was utilized. The HaCaTs were seeded in 24-well plates at a density of 2×10^5 cells per well, returned to the incubator for 24 h, then dosed with 15 μg/mL AuNPs for 24 h. The HaCaTs were washed, detached from the plate with trypsin, and fixed in 2 % paraformaldehyde/2 % glutaraldehyde. The cells were then stained with 1 % osmium tetroxide, dehydrated with increasing ethanol concentrations, and cured in 100 % LR White resin (Electron Microscopy Sciences). The pellets were then thin-sectioned using a Leica ultramicrotome and TEM imaged.

Visualization of the nano-cellular interface

The nano-cellular interface was imaged using a combination of high-resolution fluorescence and dark-field microscopy. HaCaTs were plated into a two-chambered slide at a concentration of 2×10^5 cells per chamber and allowed time to fully adhere. The cells were then exposed to either AuNPs or EGF-AuNPs under both static and dynamic conditions for 24 h. The HaCaTs were then washed, fixed with 4 % paraformaldehyde, permeabilized with Triton X-100, blocked with bovine serum albumin, and stained with DAPI and Alexa Fluor 555-phalloidin (Invitrogen) for nuclear and actin visualization. The HaCaT samples were then imaged on an Olympus BX41 microscope (fluorescence) with a CytoViva attachment (dark field) for AuNP visualization (Aetos Technologies).

Statistical analysis

All data are expressed as the mean ± the standard error of the mean. For NP agglomerate size analysis, a two-way ANOVA with Bonferroni post-test was run using Graph Pad Prism ($n = 3$, $p < 0.05$), with * indicating significance between fluids for the same NP set and † indicating significance between NP sets in the same fluid. For protein

concentration and deposition efficiency a one-way ANOVA with Bonferroni post-test was carried out ($n = 4$, $p < 0.05$) with * designating statistical significance as indicated.

Results

Gold nanoparticle selection and characterization

The nano-gold utilized in biomedical applications can span multiple morphologies, sizes, and surface coatings; each with their own advantages and disadvantages. While a number of different morphologies can be synthesized, including spheres, shells, rods, and cubes, non-spherical shapes have been associated with increased cytotoxicity (DeBrosse et al. 2013). With regards to size, previous studies have shown that 10 nm or smaller particles have greater rates of cellular internalization, as they can enter a cell through both direct diffusion and endocytosis mechanisms (Shang et al. 2014). Lastly, AuNPs naturally form a citrate coating during synthesis, meaning no additional functionalization is necessary, thereby allowing for ease of corona formation. Weighing these considerations, 10-nm spherical, citrate-coated AuNPs were the nanomaterial selected for this proof-of-concept study.

Over its years in existence, the field of nanotechnology has recognized that minor changes in NP physical properties substantially modifies particle behavior and cellular response (Hussain et al. 2015). Therefore, prior to cellular exposure the 10-nm AuNPs were fully characterized. TEM analysis was carried out (Fig. 1a) and confirmed spherical morphology of the NPs and was used to determine the primary particle size of 11.2 nm. Next, the AuNP spectral signature was identified through UV–VIS analysis, which demonstrated a single, sharp peak at approximately 520 nm (Fig. 1b). A peak at this wavelength is typical for colloidal gold and the well-defined spectral profile, in addition to TEM images, confirmed AuNP quality. As it is established that all NPs will agglomerate to some degree in solution, an initial agglomerate size in water was determined using DLS (Table 1). Lastly, surface charge of the AuNPs was identified using zeta potential, and found to be −25 mV which is typical for citrate coatings.

Generation of the EGF corona and AuNP behavior

The next goal was to generate an EGF protein corona around the AuNPs (EGF-AuNPs) and evaluate if these particles behaved differently from stock AuNPs. As exposure to the large protein source in cell media will likely modify the protein corona and AuNP behavior, characterization was carried out in both water and media environments. In water, EGF-AuNPs displayed an agglomerate size double that of untreated AuNPs; 37 nm versus 19 nm (Fig. 2a). As the presence of a protein corona increases the effective size, this diameter alteration indicated that EGF was successfully bound to the NP surface.

Following dispersion in media, the stock AuNP agglomerate size increased over four times versus the water value. This AuNP agglomeration was not surprising as the ionic content of media is known to induce NP aggregation (Sethi et al. 2009). Interestingly, the DLS data indicated that the EGF-AuNP agglomerate size did not vary between water and media environments. As NPs have almost always demonstrated increased inter-particle agglomeration following media exposure, these results suggest that the preformed EGF corona was able to alter AuNP behavior. The negligible change in aggregate sizing is likely due to the fact that the initial EGF hard corona formed a protective

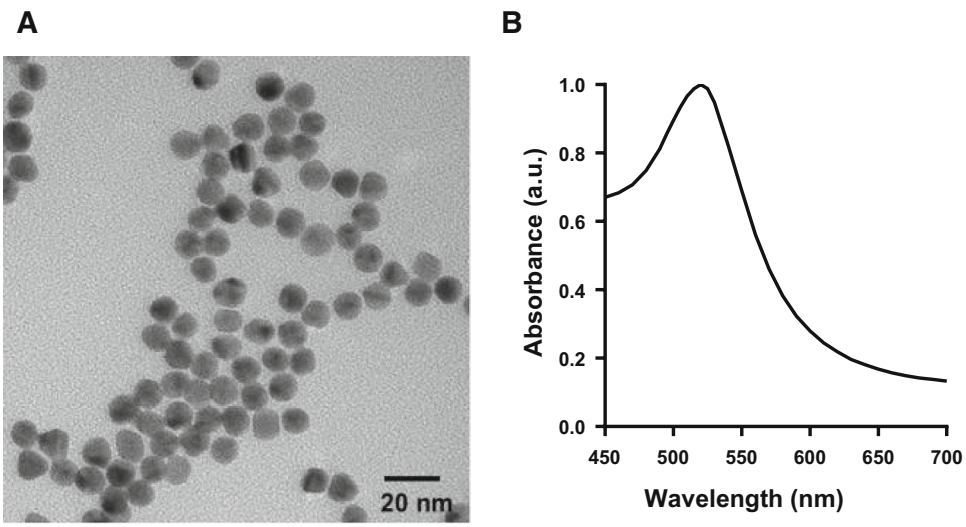

Fig. 1 **a** Representative TEM image of the 10-nm AuNPs were used to calculate a primary particle size, verify spherical morphology, and to guarantee particle uniformity. **b** The UV–VIS spectral profile of the original AuNPs demonstrated one sharp plasmonic peak at approximately 520 nm, indicative of mono-dispersed nano-sized gold particles

Table 1 Characterization of stock 10-nm AuNPs

Primary size (nm)	11.2 ± 0.8
Agglomerate size (nm)	19.3 ± 0.4
Zeta potential (mV)	−25.3 ± 2.5

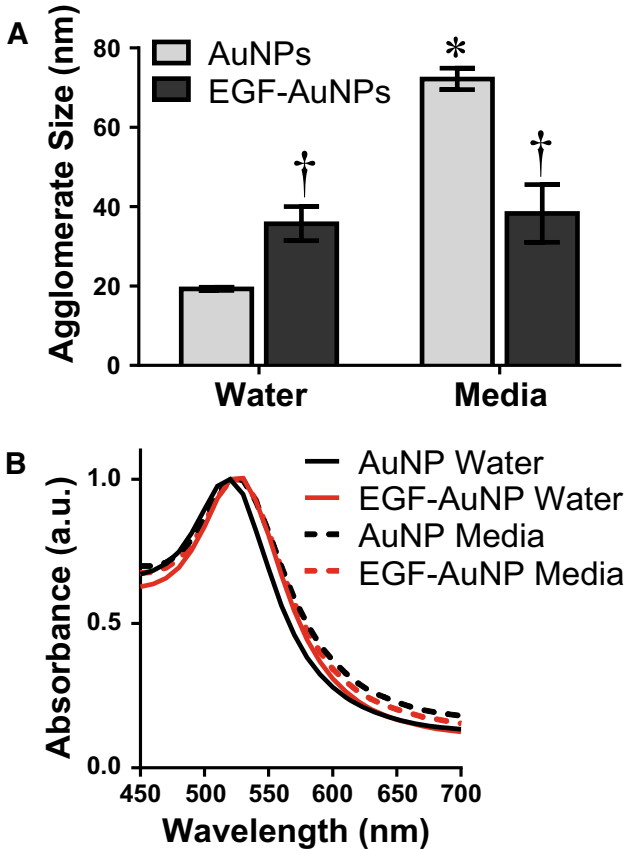

Fig. 2 **a** Agglomerate size of the AuNP sets in both water and media was assessed using dynamic light scattering. These results demonstrate the formation of a corona for EGF-AuNPS by the size increase in water. Additionally, these data identified the increased stability of the EGF-AuNPs through maintaining a constant agglomerate size following dispersion in media ($n = 3$, $p < 0.05$, with * and † indicating significance between fluids for the same NP set and between NP sets in the same fluid, respectively). **b** The UV–VIS spectral profiles of both AuNP sets following dispersion in water and media demonstrated a slight right shift and peak broadening associated with protein addition and NP agglomeration

buffer between the AuNPs and the high ionic content of the media, thus stabilizing the particles.

Next, the spectral profiles for the original and EGF-AuNPs were generated in both water and media (Fig. 2b). These profiles revealed a slight right shift in the spectral peak for EGF-AuNPs in water. This peak shift is indicative of increased AuNP agglomerate size, in agreement with the DLS data. Furthermore, a nearly identical alteration to the spectral profile was seen with both particle sets in media. In addition to the peak shift, minor broadening was identified following media exposure; suggesting a greater degree of agglomeration (Sethi et al. 2009). Taken together, the DLS and UV–VIS analyses demonstrated that the EGF-AuNPs exhibited unique behavior and physical characteristics.

To verify formation of the initial EGF corona and evaluate final corona composition in media, SDS-PAGE analysis was performed (Fig. 3a). In water, stock AuNPs displayed no associated proteins (lane 1), whereas EGF-AuNPs are associated with one predominant protein band (lane 2); visually confirming the presence of the EGF corona. As anticipated, AuNPs developed a large corona comprised of numerous proteins following exposure to media (lane 3). When examining the SDS-PAGE profile of the EGF-AuNPs in media (lane 4), several key results are observed. First, as FBS contains a large number of growth factors and cytokines, most of which have similar molecular weights, it is impossible to distinguish final EGF concentration from this analysis. Additionally, the corona

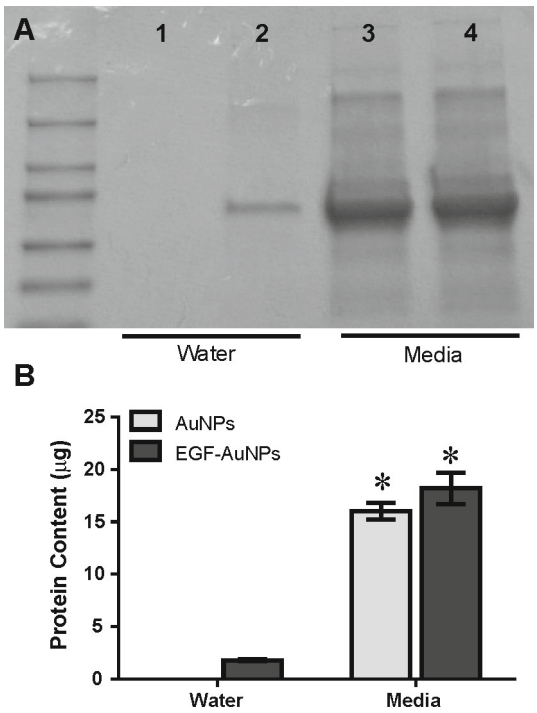

Fig. 3 **a** SDS-PAGE analysis was used to visualize the protein corona associated with (*1*) AuNPs in water, (*2*) EGF-AuNPs in water, (*3*) AuNPs in media, and (*4*) EGF-AuNPs in media. The presence of predominant, single band in *lane 2* verifies the formation of the EGF corona. **b** The protein content associated with the protein–NP complex was evaluated for all conditions and identified that in media, the EGF-AuNPs contained a larger protein corona than their untreated AuNP counterparts (n = 3, $P < 0.05$, with * indicating significance from the same AuNP condition in water)

size substantially increased in media versus water, as indicated through the rise in the number and intensity of protein bands; demonstrating an environmental dependency to the final protein–NP complex.

Next, the AuNP and EGF-AuNP protein coronas in media were directly compared. Using ImageJ software, the density of the SDS-PAGE bands was analyzed (data not shown), and identified that the EGF-AuNP bands were 17 % denser than the stock AuNPs. To verify these results, the protein content within the corona–NP complex was quantified for all experimental conditions (Fig. 3b). These results confirmed the SDS-PAGE conclusions, proving that the EGF-AuNPs bound more protein than untreated AuNPs. As the SDS-PAGE was loaded by equal NP number, final protein concentration was directly proportional to the corona size.

Evaluation of AuNP bioeffects and the nano-cellular interface

Following identification that a preliminary protein corona was able to modify both AuNP properties and the corona–NP complex, we next explored if particle delivery and biocompatibility were likewise impacted. As shown in Fig. 4a, after a 24-h exposure, the deposition rate of the EGF-AuNPs was approximately 15 % greater than the stock AuNPs. These results were the first to identify that the design and formation of a preliminary protein corona could increase the rate of NP–cellular interactions. While 15 % may not appear to be a substantial increase, this phenomena does shift the dosimetry paradigm by uncovering a mechanism that allows for some control over deposited NP dose.

Generally speaking, nano-gold is biocompatible and not does induce significant stress or cytotoxic responses. However, previous reports have directly correlated NP deposition to cell viability (Kang et al. 2013). Therefore, as the EGF-AuNPs deposited to a greater extent we assessed whether these particles induced cell toxicity following a 24-h exposure. Even though both sets of AuNPs were deposited to a large degree, no acute cellular death was identified (Fig. 4b).

NPs are typically internalized through a combination of unique endocytosis mechanisms, following membrane association (Untener et al. 2013). As the preliminary protein corona was comprised of EGF, we next investigated if the possibility of augmented EGF–EGF receptor couplings would influence AuNP internalization patterns. As seen in Fig. 5, both the stock AuNPs (Fig. 5a) and the EGF-AuNPs (Fig. 5b) were internalized with high efficiency; as evidenced through the large number of endosomes containing particles. While no distinct differences in internalization patterns were noted between AuNP sets, these images confirm that the particles were taken up through endocytosis.

Influence of dynamic flow

Next, we incorporated dynamic flow to mimic fluid movement as seen in in vivo systems. Capillaries run through skin tissue, thus generating a means for fluid movement into and out of skin cells through a combination of biological transport mechanisms. The incorporated pump system was designed to match this behavior with tube velocities set to capillary rates, producing flow across the HaCaT surface orders of magnitude lower; equivalent to diffusion and facilitated transport rates (Berger et al. 1996). Following establishment of a biologically relevant flow system, we examined how this influence varied AuNP deposition and the nano-cellular interface.

Under the influence of fluid flow, the deposition rate was significantly reduced, for both stock and EGF-coated AuNPs (Fig. 6a); with a final delivered dose only

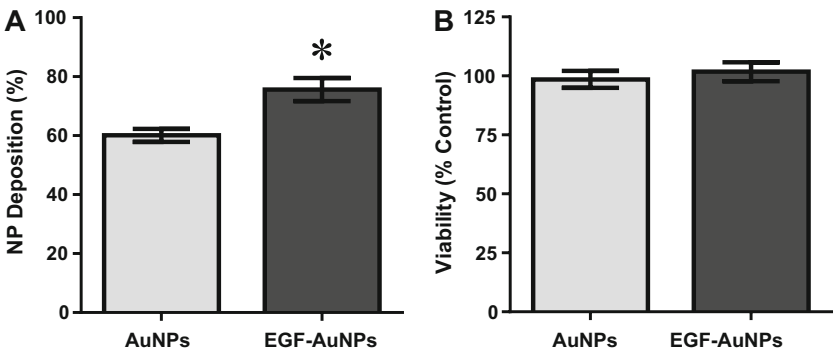

Fig. 4 **a** Under static conditions, the deposition efficiency was quantified within an HaCaT model, with a 15 % increase seen with EGF-AuNPs. **b** To ensure the biocompatibility of both AuNP sets, HaCaT cells underwent a viability assessment following a 24-h exposure. For both stock AuNPs and EGF-AuNPs, no cytotoxicity was observed ($n = 3$, $p < 0.05$, with * indicating significance between NP sets)

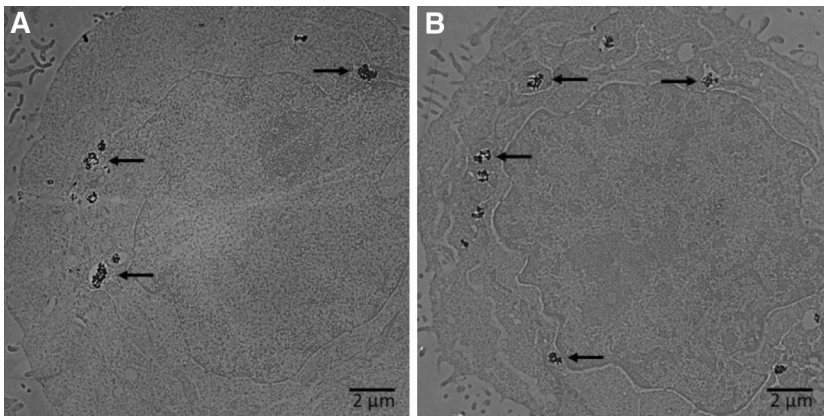

Fig. 5 Using TEM imaging, AuNP internalization within the HaCaT cell line was verified for the (**a**) stock AuNPs and (**b**) EGF-AuNPs. In these images, clusters of AuNPs are clearly identifiable within cellular endosomes. In each image, several of these NP-containing endosomes are indicated by *arrows*

approximately 35 % of administered AuNPs. The ability of dynamic flow to disrupt NP deposition has been previously seen, making these results unsurprising (Breitner et al. 2015). However, the increased deposition rate seen with EGF-AuNPs under static conditions was negated by dynamic flow. These results suggest that while the formation of a preliminary protein corona does have the potential to impact dosimetry, other physiological variables need to be accounted for during the design process.

To ensure that this observed drop in deposition was not due to HaCaT toxicity, cell viability was again assessed, this time under dynamic flow. The viability assessment showed a slight reduction in the number of live cells between dynamic and static conditions (Fig. 6b), but no significant cytotoxicity. We hypothesize that this slight reduction is due to a slower proliferative rates instead of cellular death, as has been previously seen (Gatonguay et al. 2012). Additionally, these results confirmed that the fluid movement did not negatively impact the system or induce a synergistic response with the AuNPs.

This study demonstrated that the introduction of both a preliminary EGF corona and dynamic flow altered the nano-bio interface, as evidenced through NP characterization and deposition efficiency. In an effort to better understand our observed results, our last goal was to visualize this interface, thereby producing a snapshot of NP–cellular interactions. Representative images of the nano-cellular interface for HaCaT exposure to AuNPs or EGF-AuNPs in both static and dynamic environments are shown in Fig. 7. Under static conditions (Fig. 7a, b), HaCaT morphology is primarily globular with minor actin filaments protruding. While both images demonstrate effective NP–HaCaT association, the EGF-AuNPs appear in larger clusters, suggesting higher rates of deposition and internalization; in agreement with our previous data.

Under dynamic flow (Fig. 7c, d), there is a dramatic shift in HaCaT morphology, with both the actin and nuclei elongated in the directionality of flow (left to right across image pane). These morphological alterations are not surprising, however, given that low rates of shear stress were present in the system. In addition to viewing changes to morphology, these images verify HaCaT health under dynamic flow. Taken together, the results generated in this study demonstrate that it is possible to introduce fluid dynamics to in vitro systems and that these variations have wide reaching implications including cell morphology and dosimetry.

Discussion

This proof-of-concept work successfully demonstrated the plausibility of generating a protein–NP complex prior to biological exposure in an effort to modify NP behavior and improve delivery rate. In this study, an EGF protein corona

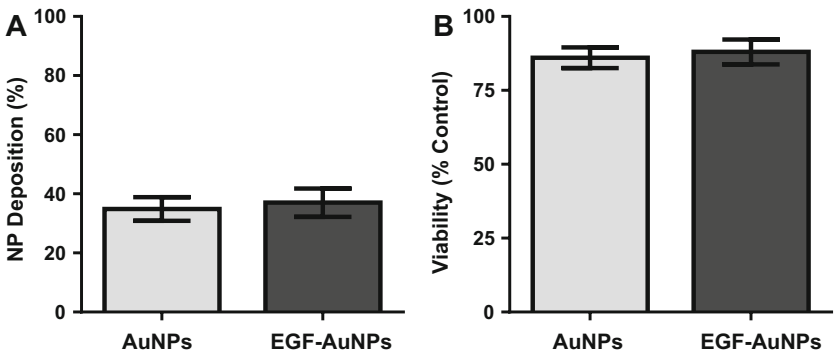

Fig. 6 Evaluation of (**a**) NP deposition efficiency and (**b**) HaCaT viability following 24-h exposure to the AuNP sets were repeated under dynamic flow conditions. These data sets suggest that the presence of flow was not harmful to the HaCaTs; however, it did severely disrupt AuNP biotransport mechanisms and final deposition efficiency

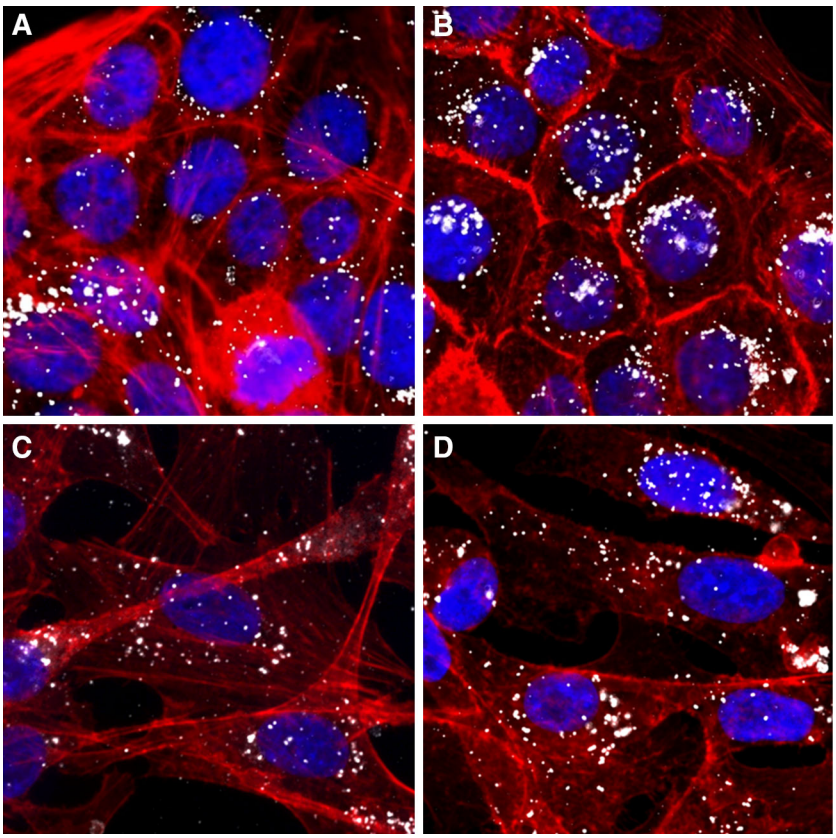

Fig. 7 Using a combination of fluorescence and dark-field microscopy, the nano-cellular interface was visualized for (**a**) AuNPs and (**b**) EGF-AuNPs under static conditions and (**c**) AuNPs and (**d**) EGF-AuNPs under dynamic flow. In addition to verifying the strong interactions between NPs and their surrounding environment, these images identified that dynamic flow altered HaCaT morphology

was successfully formed around 10-nm AuNPs. In addition to its surface receptors, EGF was specifically selected because of its documented interactions with NPs (Comfort et al. 2014b). EGF-AuNPs displayed modified behavior and an altered protein corona as compared to stock AuNPs; verifying our prediction. The presence of the EGF corona resulted in maintaining an agglomerate size of approximately 35 nm, regardless of fluid environment. As a hard protein corona was in place, the AuNPs were protected from the ionic media, thereby remaining more mono-disperse in solution and avoiding excess agglomeration. Moreover, the corona associated with the EGF-AuNPs was approximately 12 % larger than the stock AuNPs. This is likely due to their smaller agglomerate size of the EGF-AuNPs, which produces a larger surface area to volume ratio and allows for greater protein loading.

By pre-coating 10-nm AuNPs with EGF, particle deposition in an HaCaT model was increased 15 % under static conditions. While 15 % may seem minor, it is important to recall that this was a first in kind experiment and that these results successfully demonstrated that it was possible to improve the deposited NP dose through design of a protein corona. We hypothesize that this alteration to AuNP dosimetry is due to the increased particle stability and observed alteration to the protein corona. As smaller agglomerates allow for increased diffusion and NP transport, a greater fraction of AuNPs will reach the HaCaT surface (Cho et al. 2011; Hinderliter et al. 2010); thus increasing the deposition efficiency. This theory is further supported by the dynamic results, which introduced a new mode of NP transport and interfered in deposition. The presence of lateral bulk movement is traditionally stronger than diffusion, making it the primary mode of NP transport, thus diminishing NP–cellular interactions and deposition. While EGF-AuNPs displayed augmented deposition under static conditions, the presence of fluid dynamics significantly altered dosimetry, highlighting an area that is in need of further investigation.

Through visualization of the nano-cellular interface, the strong association of AuNPs and HaCaT cells was confirmed. Furthermore, AuNP internalization through endocytosis was confirmed via TEM imaging. Flow-induced modulations to cell morphology were observed, with significant actin elongation in the direction of flow, in agreement with the application of low levels of shear stress (Breitner et al. 2015). In addition to altering the mode of NP transport, altered cellular morphology will likely impeded AuNP association and internalization through disruption of the surface membrane. We believe that the observed drop in deposition under dynamic flow arises from the combination of modified modes of biotransport and reconfiguration of the HaCaT membrane structure.

Taken together, this highlights the possibility of improving NP deposition through targeted design of the protein corona; however, to make this change effective it must overcome physiological challenges, such as fluid dynamics.

Conclusion

Colloidal AuNPs hold tremendous potential to progress current technologies in the biomedical sector, but are currently limited by dosimetry capabilities. This study sought to explore if the rate of AuNP deposition and interactions in an HaCaT cell model could be improved through the targeted design of an EGF protein corona prior to biological exposure. Our results demonstrated that it was possible to generate an initial protein–NP complex and that these AuNPs displayed modulated characteristics from stock AuNPs, including greater particle stability and altered corona composition. These observed changes to AuNP physicochemical characteristics resulted in an improved deposition efficiency and altered nano-cellular interface, under static conditions. However, the introduction of dynamic flow altered AuNP transport mechanisms, thereby decreasing deposition and negating the previously seen gains by EGF-AuNPs. Therefore, this proof-of-concept work successfully demonstrated the plausibility and potential of utilizing the protein corona as a means to design and influence NP dosimetry; potentially improving effectiveness of AuNP-based biomedical applications. However, to effectively implement these modification in a physiological environment, much work remains to better understand and account for critical biological variables, such as dynamic flow.

Acknowledgments The authors would like to acknowledge the University of Dayton School of Engineering and the Dayton Area Graduate Studies Institute (DAGSI) for their financial support. The authors thank Dr. Saber M Hussain for use of his Malvern Zetasizer and fluorescence/dark-field microscope.

References

Bannunah AM, Vllasaliu D, Lord J, Stolnik S (2014) Mechanisms of nanoparticle internalization and transport across an intestinal epithelial cell model: effect of size and surface charge. Mol Pharm 11:4363–4373. doi:10.1021/mp500439c

Berger SA, Goldsmith W, Lewis ER (1996) Introduction to bioengineering. Oxford University Press, Oxford

Breitner EK, Hussain SM, Comfort KK (2015) The role of biological fluid and dynamic flow in the behavior and cellular interactions of gold nanoparticles. J Nanobiotechnol 13:56. doi:10.1186/s12951-015-0117-1

Chanana M, Rivera-Gil P, Correa-Duarte MA, Liz-Marzán LM, Parak WJ (2013) Physicochemical properties of protein-coated gold nanoparticles in biological fluids before and after proteolytic digestion. Angew Chem Int Ed Engl 52:4179–4183. doi:10.1002/anie.201208019

Cho EC, Zhang Q, Xia Y (2011) The effect of sedimentation and diffusion on cellular uptake of gold nanoparticles. Nat Nanotechnol 6:385–391. doi:10.1038/nnano.2011.58

Cichocki M, Szaefer H, Krajka-Kuzniak V, Baer-Dubowska W (2014) The effect of resveratrol and its methylthio-derivatives on EGFR and Stat3 activation in human HaCaT and A431 cells. Mol Cell Biochem 396:221–228. doi:10.1007/s11010-014-2157-5

Comfort KK, Braydich-Stolle LK, Maurer EI, Hussain SM (2014a) Less is more: long-term in vitro exposure to low levels of silver nanoparticles provides new insights for nanomaterial evaluation. ACS Nano 8:3260–3271. doi:10.1021/nn5009116

Comfort KK, Maurer EI, Hussain SM (2014b) Slow release of ions from internalized silver nanoparticles modifies the epidermal growth factor signaling response. Coll Surf B Biointerfaces 123:136–142. doi:10.1016/j.colsurfb.2014.09.008

DeBrosse MC, Comfort KK, Untener EA, Comfort DA, Hussain SM (2013) High aspect ratio gold nanorods displayed augmented cellular internalization and surface chemistry mediated cytotoxicity. Mater Sci Eng, C 33:4094–4100. doi:10.1016/j.msec.2013.05.056

Dykman L, Khlebtsov N (2012) Gold nanoparticles in biomedical applications: recent advances and perspectives. Chem Soc Rev 41:2256–2282. doi:10.1039/C1CS15166E

Gastonguay A, Berg T, Hauser AD, Schuld N, Lorimer E, Williams CL (2012) The role of Rac1 in the regulation of NF-κB activity, cell proliferation, and cell migration in non-small cell lung carcinoma. Cancer Biol Ther 13:647–656. doi:10.4161/cbt.20082

Gunawan C, Lim M, Marquis CP, Amal R (2014) Nanoparticle–protein corona complexes govern the biological fates and functions of nanoparticles. J Mat Chem B 2:2060–2083. doi:10.1039/C3TB21526A

Hamad-Schifferli (2013) How can we exploit the protein corona? Nanomedicine 8:1–3. doi:10.2217/nnm.12.179

Hinderliter PM, Minard KR, Orr G et al (2010) ISDD: a computational model of particle sedimentation, diffusion, and target cell dosimetry for in vitro toxicity studies. Part Fibre Toxicol 7:36. doi:10.1186/1743-8977-7-36

Hussain SM, Warheit DB, Ng SP, Comfort KK, Grabinski CM, Braydich-Stolle LK (2015) At the crossroads of nanotoxicology in vitro: past achievements and current challenges. Toxicol Sci 147:5–16. doi:10.1093/toxsci/kfv106

Kang M, Lim CH, Han JH (2013) Comparison of toxicity and deposition of nano-sized carbon black aerosol prepared with and without dispersing sonication. Toxicol Res 29:121–127. doi:10.5487/TR.2013.29.2.121

Kusunose J, Zhang H, Gagnon MK, Pan T, Simon SI, Ferrara KW (2013) Microfluidic system for facilitated quantification of nanoparticle accumulation to cells under laminar flow. Ann Biomed Eng 41:89–99. doi:10.1007/s10439-012-0634-0

Lesniak A, Salvati A, Santos-Martinez MJ, Radomski MW, Dawson KA, Aberg C (2013) Nanoparticle adhesion to the cell membrane and its effect on nanoparticle uptake. J Am Chem Soc 135:1438–1444. doi:10.1021/ja309812z

Pal A, Bello D, Cohen J, Demokritou P (2015) Implications of in vitro dosimetry on toxicological ranking of low aspect ratio engineered nanomaterials. Nanotoxicology 12:1–15. doi:10.3109/17435390.2014.986670

Sahneh FD, Scoglio CM, Monteiro-Riviere NA, Riviere JE (2015) Predicting the impact of biocorona formation kinetics on interspecies extrapolations of nanoparticle biodistribution modeling. Nanomedicine 10:25–33. doi:10.2217/nnm.14.60

Salvati A, Pitek AS, Monopoli MP et al (2013) Transferrin-functionalized nanoparticles lose their targeting capabilities when a biomolecule corona adsorbs on the surface. Nat Nanotechnol 8:137–143. doi:10.1038/nnano.2012.237

Sethi M, Joung G, Knecht MR (2009) Stability and electrostatic assembly of Au nanorods for use in biological assays. Langmuir 25:317–325. doi:10.1021/la802096v

Shang L, Nienhaus K, Nienhaus GU (2014) Engineered nanoparticles interacting with cells: size matters. J Nanobiotechnol 12:5. doi:10.1186/1477-3155-12-5

Stacy BM, Comfort KK, Comfort DA, Hussain SM (2013) In vitro identification of gold nanorods through hyperspectral imaging. Plasmonics 8:1235–1240. doi:10.1007/s11468-013-9538-6

Tenzer S, Docter D, Kuharev J et al (2013) Rapid formation of plasma protein corona critically affects nanoparticle pathophysiology. Nat Nanotechnol 8:772–781. doi:10.1038/nnano.2013.181

Treuel L, Brandholt S, Maffre P, Wiegele S, Shang L, Nienhaus GU (2014) Impact of protein modification on the protein corona on nanoparticles and nanoparticle–cell interactions. ACS Nano 8:503–513. doi:10.1021/nn405019v

Ucciferri N, Collnot EM, Gaiser BK, Tirella A, Stone V, Domenici C, Lehr CM, Ahluwalia A (2014) In vitro toxicological screening of nanoparticle on primary human endothelial cells and the role of flow in modulating cell response. Nanotoxicology 8:697–708. doi:10.3109/17435390.2013.831500

Untener EA, Comfort KK, Maurer EI, Grabinski CM, Comfort DA, Hussain SM (2013) Tannic acid coated gold nanorods demonstrate a distinctive form of endosomal uptake and unique distribution within cells. ACS Appl Mater Interfaces 11:8366–8373. doi:10.1021/am402848q

Winzen S, Schoettler S, Baier G, Rosenauer C, Mailaender V, Landfester K, Mohr K (2015) Complementary analysis of the hard and soft protein corona: sample preparation critically effects corona composition. Nanoscale 7:2992–3001. doi:10.1039/c4nr05982d

Yeh YC, Creran B, Rotello VM (2012) Gold nanoparticles: preparation, properties, and applications in bionanotechnology. Nanoscale 4:1871–1880. doi:10.1039/C1NR11188D

Zook JM, Long SE, Cleveland D, Geromino CL, MacCuspie RI (2011) Measuring silver nanoparticle dissolution in complex biological and environmental matrices using UV–visible absorbance. Anal Bioanal Chem 401:1993–2002. doi:10.1007/s00216-011-5266-y